RAPID COMMUNICATIONS

PHYSICAL REVIEW B **94**, 060404(R) (2016)

Spin crossover and hyperfine interactions of iron in (Mg,Fe)CO_3 ferromagnesite

Han Hsu[*] and Sheng-Chieh Huang

Department of Physics, National Central University, Taoyuan City 32001, Taiwan

(Received 6 April 2016; revised manuscript received 16 June 2016; published 8 August 2016)

Ferromagnesite, an iron-bearing carbonate stable up to 100–115 GPa, is believed to be the major carbon carrier in the earth's lower mantle and play a key role in the earth's deep carbon cycle. In this paper, we use the local density approximation plus self-consistent Hubbard U (LDA+U_{sc}) method to study the iron spin crossover in ferromagnesite with a wide range of iron concentration (12.5–100%). Our calculation shows that this mineral undergoes a crossover from the high-spin (HS) ($S = 2$) to the low-spin (LS) ($S = 0$) state at around 45–50 GPa, regardless of the iron concentration. The intermediate-spin ($S = 1$) state is energetically unfavorable and not involved in spin crossover. The anomalous changes of volume, density, and bulk modulus accompanying the spin crossover obtained in our calculation are in great agreement with experiments. Our calculation also predicts that an abrupt change of the iron nuclear quadrupole splitting, from $\gtrsim 2.8$ mm/s to $\lesssim 0.3$ mm/s, can be observed in Mössbauer spectra at 45–50 GPa as a signature of the HS-LS crossover.

DOI: 10.1103/PhysRevB.94.060404

Iron-bearing magnesium carbonates [(Mg,Fe)CO_3] have attracted significant attention in recent years; they are believed to be the major carbon carrier in the earth's lower mantle (660–2890 km deep, in the pressure range 23–135 GPa) and play a key role in the earth's deep carbon cycle [1]. Experiments have shown that ferromagnesite, a solid solution of $MgCO_3$ magnesite and $FeCO_3$ siderite (both crystallizing in $R\bar{3}c$ symmetry, space group No. 167), is the stable phase of (Mg,Fe)CO_3 up to 100–115 GPa [1,2]. Beyond this pressure, ferromagnesite undergoes a complicated structural transition, which has been a matter of intense debate [1–7]. Several distinct structures have been inferred from experiments performed with $(Mg_{1-x},Fe_x)CO_3$ $(0.6 < x \leqslant 1)$, including two monoclinic [5,7] and two orthorhombic [2,6] structures. Currently available first-principles structural searches of high-pressure carbonates, however, are based on pure $MgCO_3$ and are unable to resolve this controversy [3,4]. Clearly, iron directly affects the structural transition of carbonates.

One more complexity caused by iron is spin crossover (SCO), namely, the total electron spin S of iron varies with pressure. A well studied example is (Mg,Fe)O ferropericlase (Fp), which constitutes ~20 vol% of the lower mantle. As the pressure increases, ferrous iron (Fe^{2+}) in Fp undergoes a crossover from the high-spin (HS) ($S = 2$) to the low-spin (LS) ($S = 0$) state at 40–50 GPa, accompanied by anomalous changes of the structural, electronic, optical, elastic, and thermodynamic properties [8–21]. So far, several experiments have indicated SCO in ferromagnesite occurring at 44–52 GPa, including the decrease of the satellite peak intensity $K\beta'$ in x-ray emission spectroscopy spectra, the change of optical absorption and Raman spectra, and the volume and elastic anomalies [22–30]. These experiments, however, cannot unambiguously determine the mechanism of SCO, in particular, whether the intermediate-spin (IS) ($S = 1$) state is involved. Given that the IS state has been a controversy in many SCO systems, including coordination complexes [31,32], bulk and thin-film $LaCoO_3$ [33–39], and earth minerals [20,40–50], and that SCO has been suggested to be a potential pathway to stabilize the uncharacterized orthorhombic $FeCO_3$ siderite II beyond 100 GPa [6], a rigorous computational study of the SCO in ferromagnesite would be a desirable first step to help elucidate the behavior of the (Mg,Fe)CO_3 system in the deep lower mantle.

Computationwise, the strongly correlated nature of iron cannot be properly treated by standard density functional theory methods, including the local density approximation (LDA) and generalized gradient approximation (GGA). For $FeCO_3$ siderite, known as an antiferromagnetic (AFM) insulator at ambient pressure [51], the GGA falsely predicts a metallic ferromagnetic (FM) ground state [52], produces a metallic state when AFM configured [53,54], and fails to obtain the IS state [30,52–54], despite its potential importance in the (Mg,Fe)CO_3 system. Also, the effect of iron concentration on SCO is unaddressed. Here we investigate $(Mg_{1-x},Fe_x)CO_3$ ferromagnesite $(0.125 \leqslant x \leqslant 1)$ using the LDA plus self-consistent U (LDA+U_{sc}) method with the Hubbard U parameter computed from first principles (see Supplemental Material [55] and Refs. [46,56–59]), given that the LDA+U_{sc} has successfully clarified the highly controversial IS state and SCO in Fe-bearing $MgSiO_3$ perovskite (Pv) (also known as bridgmanite, constituting ~75 vol % of the lower mantle) and post-perovskite (pPv) and accurately determines the transition pressures [45–49].

In $(Mg_{1-x},Fe_x)CO_3$ ferromagnesite and its end member $FeCO_3$ siderite ($x = 1$), iron resides in a trigonally distorted octahedral site, with the FeO_6 octahedron elongating along the [111] direction, as shown in Fig. 1 (also see Supplemental Material [55]). In this crystal field (D_{3d} symmetry), the five $3d$ orbitals split into three subgroups: a doublet pointing toward the oxygen [Fig. 2(a)] and a doublet [Fig. 2(b)] and a singlet d_{z^2} [Fig. 2(c)] pointing away from the oxygen (also see Supplemental Material [55]). For d^6 cations, e.g., Fe^{2+} or Co^{3+}, the HS state has five majority-spin electrons occupying all $3d$ orbitals and one minority-spin electron occupying the singlet d_{z^2} [Fig. 2(c)]; the LS state has all six electrons doubly occupying the three orbitals pointing away from the oxygen [Figs. 2(b) and 2(c)], leading to a nearly-cubic-shaped electron charge density schematically shown in Fig. 2(d). The IS state has two minority-spin electrons occupying the doublet shown in Fig. 2(b), leading to the

---

[*] hanhsu@ncu.edu.tw

©2016 American Physical Society

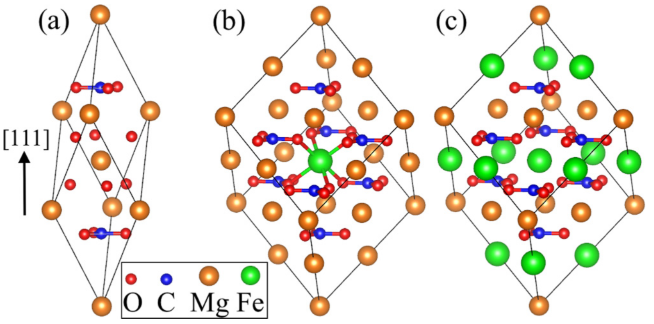

FIG. 1. Crystal structure of $(\mathrm{Mg}_{1-x},\mathrm{Fe}_x)\mathrm{CO}_3$ ferromagnesite. The orange, green, blue, and red spheres are Mg, Fe, C, and O atoms, respectively. (a) Ten-atom primitive cell of MgCO_3 magnesite ($R\bar{3}c$ symmetry). (b) and (c) 40-atom supercells with $x = 0.125$ and 0.5, respectively.

electron charge density schematically shown in Fig. 2(e); its four majority-spin electrons fully occupy the three orbitals shown in Figs. 2(b) and 2(c) and half occupy the doublet pointing toward the oxygen [Fig. 2(a)]. The self-consistent Hubbard U of these states are computed using 40-atom $(\mathrm{Mg}_{0.875},\mathrm{Fe}_{0125})\mathrm{CO}_3$ supercells at 0 and 100 GPa. The resultant U_{sc} mainly depends on the iron spin state and marginally increases with pressure, by ∼0.5 eV throughout 0–100 GPa. We thus adopt the average: $U_{\mathrm{sc}}^{(HS)} = 4.0$, $U_{\mathrm{sc}}^{(IS)} = 5.7$, and $U_{\mathrm{sc}}^{(LS)} = 5.3$ eV. In ferromagnesite, $U_{\mathrm{sc}}^{(HS)}$ is the lowest among the three U_{sc}, similar to Fp, Fe-bearing Pv/pPv, and thin-film LaCoO_3 [35,45–50].

The LDA+U_{sc} electronic structures of HS and IS $(\mathrm{Mg}_{0.875},\mathrm{Fe}_{0125})\mathrm{CO}_3$ at ∼60 GPa are shown in Figs. 3(a) and 3(c), respectively; the total and projected density of states (PDOS) on each atomic site are plotted, with the Fermi level E_F shifted to 0 eV (see Supplemental Material [55] for the LS state). As is evident from Fig. 3(a), HS $(\mathrm{Mg}_{0.875},\mathrm{Fe}_{0125})\mathrm{CO}_3$ is an insulator with a finite gap. Also, several PDOS peaks resulting from Fe can be observed. In the spin-up channel, the PDOS peaks at −1.4 and −2.9 eV correspond to the doublet shown in Fig. 2(a) and the singlet shown in Fig. 2(c), respectively. The doublet pointing away from oxygen [Fig. 2(b)] forms a wide band between −3.5 and −7.8 eV instead of a PDOS peak. In the spin-down channel, the only Fe PDOS peak (at −1.3 eV) corresponds to the singlet [Fig. 2(c)]. The association

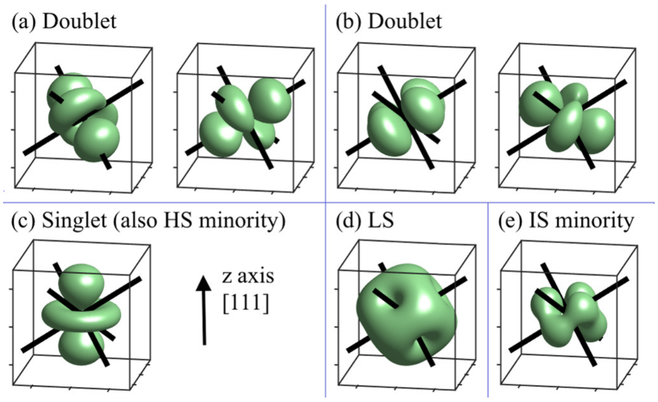

FIG. 2. (a)–(c) The 3d orbitals in a trigonally distorted crystal field (D_{3d} symmetry). The black thick segments represent the Fe-O bonds; the [111] direction is aligned with the z axis. (d) Sum of the three occupied orbitals [panels (b) and (c)] of the LS Fe^{2+}. (e) Sum of the two orbitals occupied by the monitory-spin electrons of the IS Fe^{2+} [panel (b)]. The minority-spin electron of the HS Fe^{2+} occupies the singlet [panel (c)].

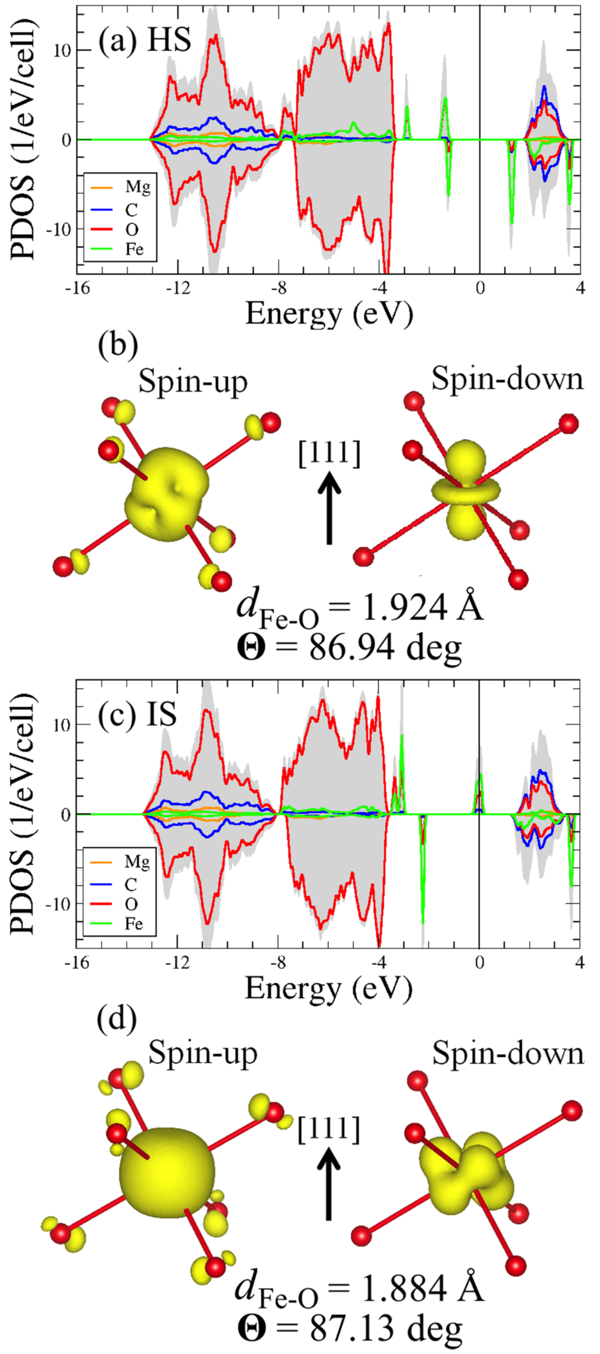

FIG. 3. Electronic structures of high-spin and intermediate-spin $(\mathrm{Mg}_{0.875},\mathrm{Fe}_{0.125})\mathrm{CO}_3$ at ∼60 GPa (40-atom supercell with $V = 274.47$ Å^3). (a) and (c) Total (gray shade) and projected density of states on each atomic site (lines) of the HS and IS states, respectively. (b) and (d) Integrated local density of states of the Fe peaks in (a) and (c), respectively (isosurface of 0.05 a.u.$^{-3}$). The Fe-O bond length $d_{\text{Fe-O}}$ and O-Fe-O bond angle Θ are also indicated.

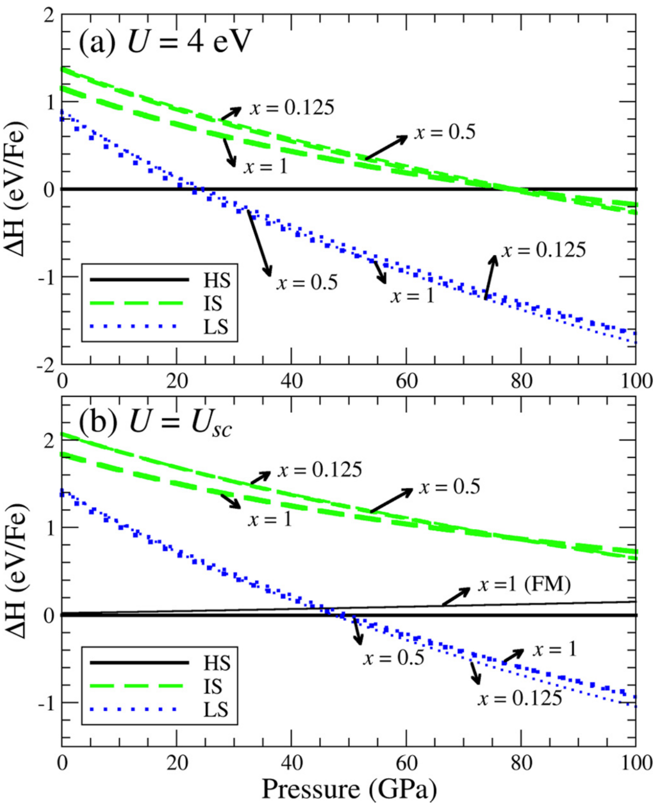

FIG. 4. Relative enthalpy ΔH of IS and LS $(\mathrm{Mg}_{1-x},\mathrm{Fe}_x)\mathrm{CO}_3$ ferromagnesite with respect to the HS state. Calculations with (a) $U = 4$ eV and (b) self-consistent U_{sc} are shown ($U_{\mathrm{sc}}^{(HS)} = 4.0$, $U_{\mathrm{sc}}^{(IS)} = 5.7$, and $U_{\mathrm{sc}}^{(LS)} = 5.3$ eV). The solid, dashed, and dotted lines represent the HS, IS, and LS states, respectively; different linewidths represent different iron concentrations $x = 0.125$, 0.5, and 1. For FeCO_3 siderite ($x = 1$), the ground state is an AFM-ordered HS state; the FM-ordered HS state has a slightly higher enthalpy, as shown in (b).

of these PDOS peaks with the $3d$ orbitals is consistent with the integrated local density of states[1] (ILDOS) shown in Fig. 3(b). Based on Fig. 3(c), the IS state has a half-metallic electronic structure with a PDOS peak at the Fermi level due to the half-occupied doublet, similar to the half-metallic IS state of bulk LaCoO_3 ($R\bar{3}c$ symmetry) [34]. The spin-down PDOS peak at -2.2 eV corresponds to the doublet pointing away from the oxygen, which is evident by comparing Fig. 3(d) with Fig. 2(e). The HS and IS states distort the Fe-O octahedron differently. As indicated in Figs. 3(b) and 3(d), the HS state leads to a greater Fe-O bond length ($d_{\text{Fe-O}}$) and a smaller O-Fe-O bond angle Θ.

To investigate SCO and its composition dependence, the enthalpies of $(\mathrm{Mg}_{1-x},\mathrm{Fe}_x)\mathrm{CO}_3$ ferromagnesite ($x = 0.125$, 0.5, and 1) in each spin state are computed. Calculations with $U = 4$ eV and U_{sc} are performed, so the effect of the Hubbard U can be determined. For FeCO_3 siderite ($x = 1$), both choices of U predict a HS AFM insulating ground state at 0 GPa, consistent with experiments [51], while IS FeCO_3 favors FM ordering. The relative enthalpy ΔH of the LS and IS-FM states with respect to the HS-AFM state are shown in Fig. 4. As can be seen in Fig. 4(b), the enthalpy difference between the HS-FM and HS-AFM state is small and the SCO is barely affected by magnetic ordering. For $x = 0.125$ and 0.5, the alignment of spin moment does not cause any difference; only the parallel-alignment results are plotted. As shown in Figs. 4(a) and 4(b), only the HS-LS crossover occurs and the IS state is energetically unfavorable, regardless of the iron concentration and the choice of the Hubbard U (4 eV or U_{sc}). The main difference is the HS-LS transition pressure P_T. When $U = 4$ eV, $P_T = 22$–25 GPa, which is significantly lower than observed in experiments (44–52 GPa), while U_{sc} leads to $P_T = 47$–50 GPa, in great agreement with experiments [22–30]. Remarkably, both theory and experiment show that P_T barely depends on iron concentration, suggesting a weak Fe-Fe interaction in ferromagnesite, in contrast with $(\mathrm{Mg}_{1-x},\mathrm{Fe}_x)\mathrm{O}$ Fp, in which P_T significantly increases with iron concentration in the iron-rich regime ($0.5 < x < 1$) [20,29]. Such a difference can be attributed to the atomic structure of these minerals. In ferromagnesite, the Fe-O octahedra are isolated; even in FeCO_3 siderite, the Fe-O octahedra only share corners. In Fp, the Fe-O octahedra share faces when $x > 0.5$ and the Fe-Fe distance is shorter than in ferromagnesite.

At nonzero temperatures T, the spin crossover in ferromagnesite goes through a mixed-spin phase within a finite pressure range. Without including the vibrational free energy, the fraction n_i of each spin state i ($i =$ LS, IS, or HS) in the mixed-spin phase can be estimated using Eq. (1) with the constraint $\sum_i n_i = 1$ (see Refs. [17,60]),

$$\frac{n_i}{n_{HS}} = \frac{m_i(2S_i + 1)}{m_{HS}(2S_{HS} + 1)} \exp\left(-\frac{\Delta H_i}{k_B T x}\right), \tag{1}$$

where m_i and S_i are the orbital degeneracy and total electron spin of spin state i, respectively. Ferromagnesite has $m_{HS} = m_{IS} = m_{LS} = 1$, due to the rhombohedral symmetry. For $x = 0.125$, 0.65, and 1, the fraction n_i at room temperature ($T = 300$ K) is plotted in Figs. 5(a)–5(c), respectively, and the corresponding mixed-spin compression curves are plotted in Figs. 5(d)–5(f), respectively, along with the HS, IS, and LS states and experimental results [26–30]. Again, only the HS-LS crossover is observed; the IS fraction is negligible [Figs. 5(a)–5(c)]. Shown in Figs. 5(d)–5(f), the computed 300 K volume is overall 4% smaller than the measurement. This discrepancy can be reduced by the inclusion of vibrational free energy. On the other hand, the computed volume reductions accompanying the SCO are in great agreement with experiments, as can be observed in Figs. 5(g)–5(i), where the volume difference between (Mg,Fe)CO_3 and MgCO_3 is plotted, with the measured MgCO_3 compression curve [$V_{Ms}(P)$] adopted from Ref. [29] and the computed $V_{Ms}(P)$ determined with the LDA. Using $x = 0.65$ as an example [Fig. 5(h)], both theory and experiment show a volume reduction of ~7%, namely, from 3–4 % larger than to 3–4 % smaller than pure

---

[1] The integrated local density of states $I(\mathbf{r}) \equiv \int_{E_1}^{E_2} dE\, \delta(E - E_{n,\mathbf{k}})|\Psi_{n,\mathbf{k}}(\mathbf{r})|^2$, where $E_{n,\mathbf{k}}$ is the energy eigenvalue of the Bloch state $|\Psi_{n,\mathbf{k}}\rangle$. To plot the ILDOS of the HS and IS states, we set $E_1 = -3.2$ and -3.6 eV, respectively, and $E_2 = 0 \equiv E_F$. The Fe PDOS peaks below E_F shown in Figs. 3(a) and 3(c) are included in the energy interval bound by E_1 and E_2, therefore, the Fe $3d$ electron charge density is depicted in the ILDOS plots.

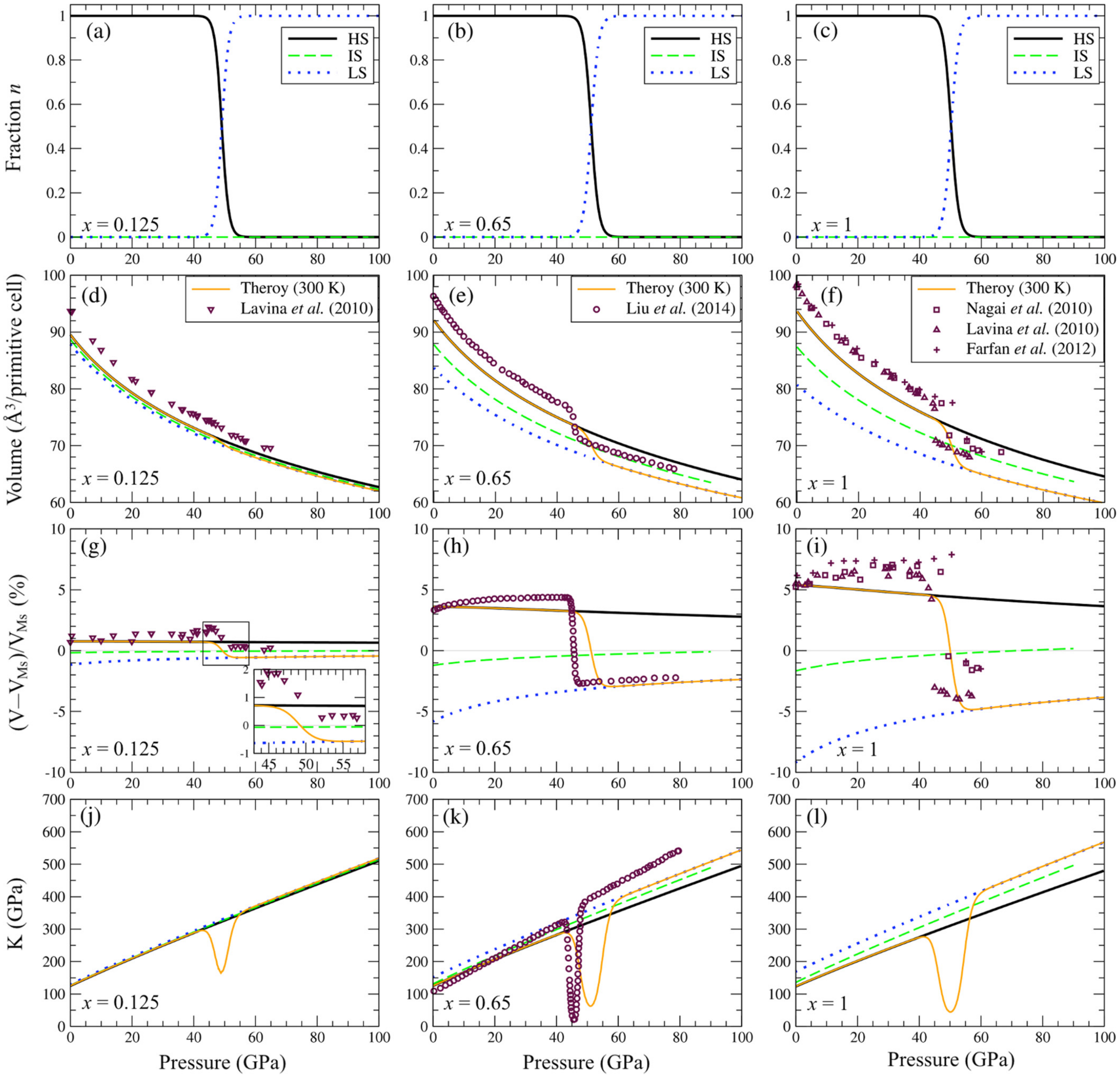

FIG. 5. Spin crossover of $(Mg_{1-x},Fe_x)CO_3$ ferromagnesite with various iron concentrations ($x = 0.125$, 0.65, and 1) and the accompanying volume reduction and elastic anomalies. (a)–(c) The fraction n_i of spin state i in the mixed-spin phase at $T = 300$ K. (d)–(f) Compression curves of each spin state and the mixed-spin phase. (g)–(i) Volume difference with respect to $MgCO_3$ magnesite (V_{Ms}). (j)–(l) Bulk modulus of each spin state and the mixed-spin phase. The black (dark solid), green (dashed), blue (dotted), and orange (light solid) lines are the HS, IS, LS, and mixed-spin states at $T = 300$ K, respectively; symbols are room-temperature measurements [26–30].

$MgCO_3$. In the other two cases ($x = 0.125$ and 1), the same level of agreement persists in terms of volume reduction. For bulk modulus K [Figs. 5(j)–5(l)], theory and experiment also show nearly the same dip starting at nearly the same pressure [Fig. 5(k)]. The main difference is the width of the HS-LS crossover: ∼5 GPa in experiment and ∼10 GPa in theory.

While the volume reduction shown in Fig. 5 provides useful information regarding SCO, a much more reliable way to unambiguously identify iron spin state is by comparing the computed and measured iron nuclear quadrupole splitting (QS), as demonstrated in Fe-bearing Pv and pPv [45–50]. Our calculation predicts that an abrupt change of QS from $\gtrsim$2.8 mm/s to $\lesssim$0.3 mm/s can be observed at 45–50 GPa as a signature of the HS-LS crossover (see Supplemental Material [55]). The IS state, with a QS of ∼1.8 mm/s, is highly unlikely.

In the earth's lower mantle, ferromagnesite could experience temperatures up to 2000–3000 K, if not dissociating or melting. The volume and elastic anomalies accompanying the SCO at high temperature, along with the fraction of

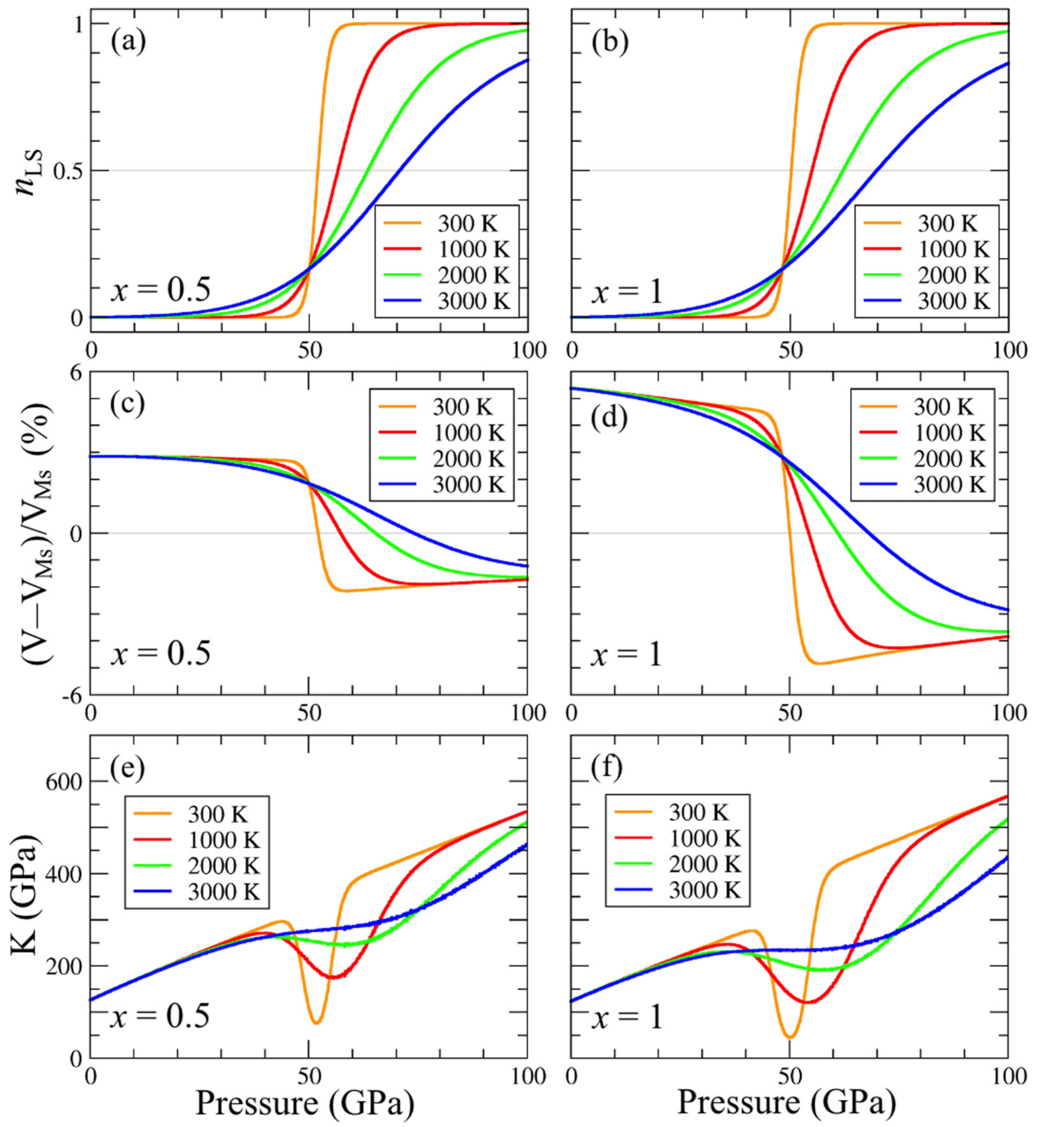

FIG. 6. Temperature effects on the spin crossover of $(Mg_{1-x},Fe_x)CO_3$ ($x = 0.5$ and 1.0) and accompanying volume and elastic anomalies. (a) and (b) The fraction of LS iron n_{LS} in the mixed-spin phase at various temperatures. (c) and (d) Volume difference with respect to $MgCO_3$ magnesite V_{Ms} at various temperatures. (e) and (f) Bulk modulus of $(Mg,Fe)CO_3$ at various temperatures.

each spin state, are estimated using Eq. (1) and plotted in Fig. 6 (with $x = 0.5$ and 1). As is evident from the LS fraction n_{LS} shown in Figs. 6(a) and 6(b) (n_{IS} is essentially zero and $n_{HS} = 1 - n_{LS}$), both the transition pressure (at which $n_{LS} = n_{HS} = 0.5$) and the width of SCO increase with temperature. Consequently, the anomalous volume reduction [Figs. 6(c) and 6(d)] and bulk modulus softening [Figs. 6(e) and 6(f)] shifts toward higher pressure and becomes smoother. Nevertheless, the volume and elastic anomalies are still prominent at $T = 2000$ K. Similar temperature effects are also observed in Fp and Fe-bearing Pv [13,15,17,20,46].

In summary, we have investigated the iron spin crossover in $(Mg_{1-x},Fe_x)CO_3$ ferromagnesite using the the LDA+U_{sc} method, from the iron-poor ($x = 0.125$) to the iron-rich ($x = 1$, $FeCO_3$ siderite) regime. Our calculation shows a high-spin to low-spin crossover at 45–50 GPa without going through the intermediate-spin state, regardless of the iron concentration. All the major calculational results, including the transition pressure, the negligible dependence of the transition pressure on the iron concentration, and the volume and elastic anomalies accompanying the HS-LS crossover, are in great agreement with experiments. Our calculation also predicts an abrupt change of the iron nuclear QS, from $\gtrsim$2.8 mm/s to $\lesssim$0.3 mm/s, at 45–50 GPa as a signature of the HS-LS crossover. These accurate results, along with the previous success in Fe-bearing $MgSiO_3$ Pv/pPv, suggest that the LDA+U_{sc} can make reliable predictions regarding the structural transition of iron-bearing carbonates in the earth's deep lower mantle, a subject of great geophysical and geochemical interest.

This work was supported by the Ministry of Science and Technology of Taiwan under Grants No. MOST 104-2112-M-008-005-MY3 and No. 103-2119-M-001-011-MY2. Some calculations were performed at the National Center for High-performance Computing of Taiwan.

[1] *Carbon in Earth*, edited by R. M. Hazen, A. P. Jones, and J. A. Baross, special issue of Rev. Mineral. Geochem. 75(1) (2013).

[2] M. Isshiki, T. Irifune, K. Hirose, S. Ono, Y. Ohishi, T. Watanuki, E. Nishibori, M. Takata, and M. Sakata, Nature (London) **427**, 60 (2004).

[3] A. R. Oganov, S. Ono, Y. Ma, C. W. Glass, and A. Garcia, Earth Planet. Sci. Lett. **273**, 38 (2008).

[4] C. J. Pickard and R. J. Needs, Phys. Rev. B **91**, 104101 (2015).

[5] E. Boulard, A. Gloter, A. Corgne, D. Antonangeli, A.-L. Auzende, J.-P. Perrillat, F. Guyot, and G. Fiquet, Proc. Natl. Acad. Sci. U.S.A. **108**, 5184 (2011).

[6] J. Liu, J.-F. Lin, and V. Prakapenka, Sci. Rep. **5**, 7640 (2015).

[7] E. Boulard, D. Pan, G. Galli, Z. Liu, and W. L. Mao, Nat. Commun. **6**, 6311 (2015).

[8] J. Badro, G. Fiquet, F. Guyot, J. Rueff, V. Struzhkin, G. Vanko, and G. Monaco, Science **300**, 789 (2003).

[9] J.-F. Lin, V. V. Struzhkin, S. D. Jacobsen, M. Y. Hu, P. Chow, J. Kung, H. Liu, H.-k. Mao, and R. J. Hemley, Nature (London) **436**, 377 (2005).

[10] S. Speziale, A. Milber, V. E. Lee, S. M. Clark, M. P. Pasternak, and R. Jeanloz, Proc. Natl. Acad. Sci. U.S.A. **102**, 17918 (2005).

[11] T. Tsuchiya, R. M. Wentzcovitch, C. R. S. da Silva, and S. de Gironcoli, Phys. Rev. Lett. **96**, 198501 (2006).

[12] A. F. Goncharov, V. V. Struzhkin, and S. D. Jacobsen, Science **312**, 1205 (2006).

[13] J.-F. Lin, G. Vanko, S. D. Jacobsen, V. Iota, V. V. Struzhkin, V. B. Prakapenka, A. Kuznetsov, and C.-S. Yoo, Science **317**, 1740 (2007).

[14] J. Crowhurst, J. M. Brown, A. F. Goncharov, and S. D. Jacobsen, Science **319**, 451 (2008).

[15] R. M. Wentzcovitch, J. F. Justo, Z. Wu, C. R. S. da Silva, D. A. Yuen, and D. Kohlstedtd, Proc. Natl. Acad. Sci. U.S.A. **106**, 8447 (2009).

[16] H. Marquardt, S. Speziale, H. J. Reichmann, D. J. Frost, F. R. Schilling, and E. J. Garnero, Science **324**, 224 (2009).

[17] H. Hsu, K. Umemoto, Z. Wu, and R. M. Wentzcovitch, Rev. Mineral Geochem. **71**, 169 (2010).

[18] D. Antonangeli, J. Siebert, C. M. Aracne, D. L. Farber, A. Bosak, M. Hoesch, M. Krisch, F. J. Ryerson, G. Fiquet, and J. Badro, Science **331**, 64 (2011).

[19] Z. Wu, J. F. Justo, and R. M. Wentzcovitch, Phys. Rev. Lett. **110**, 228501 (2013).

[20] J.-F. Lin, S. Speziale, Z. Mao, and H. Marquardt, Rev. Geophys. **51**, 244 (2013).

[21] E. Holmstrom and L. Stixrude, Phys. Rev. Lett. **114**, 117202 (2015).

[22] A. Mattila, T. Pylkkanen, J.-P. Rueff, S. Huotari, G. Vanko, M. Hanfland, M. Lehtinen, and K. Hamalainen, J. Phys.: Condens. Matter **19**, 386206 (2007).

[23] B. Lavina, P. Dera, R. T. Downs, V. Prakapenka, M. Rivers, S. Sutton, and M. Nicol, Geophys. Res. Lett. **36**, L23306 (2009).

[24] J.-F. Lin, J. Liu, C. Jacobs, and V. Prakapenka, Am. Min. **97**, 583 (2012).

[25] S. S. Lobanov, A. F. Goncharov, and K. D. Litasov, Am. Min. **100**, 1059 (2015).

[26] T. Nagai, T. Ishido, Y. Seto, D. Nishio-Hamane, N. Sata, and K. Fujino, J. Phys.: Conf. Ser. **215**, 012002 (2010).

[27] B. Lavina, P. Dera, R. T. Downs, O. Tschauner, W. Yang, O. Shebanova, and G. Shen, High Press. Res. **30**, 224 (2010).

[28] B. Lavina, P. Dera, R. T. Downs, W. Yang, S. Sinogeikin, Y. Meng, G. Shen, and D. Schiferl, Phys. Rev. B **82**, 064110 (2010).

[29] J. Liu, J.-F. Lin, Z. Mao, and V. Prakapenka, Am. Min. **99**, 84 (2014).

[30] G. Farfan, S. Wang, H. Ma, R. Caracas, and W. L. Mao, Am. Min. **97**, 1421 (2012).

[31] K. Tarafder, S. Kanungo, P. M. Oppeneer, and T. Saha-Dasgupta, Phys. Rev. Lett. **109**, 077203 (2012).

[32] W. Zhang *et al.*, Nature (London) **509**, 345 (2014).

[33] H. Hsu, K. Umemoto, M. Cococcioni, and R. M. Wentzcovitch, Phys. Rev. B **79**, 125124 (2009), and references therein.

[34] H. Hsu, P. Blaha, R. M. Wentzcovitch, and C. Leighton, Phys. Rev. B **82**, 100406(R) (2010), and references therein.

[35] H. Hsu, P. Blaha, and R. M. Wentzcovitch, Phys. Rev. B **85**, 140404(R) (2012), and references therein.

[36] W. S. Choi, J.-H. Kwon, H. Jeen, J. E. Hamann-Borrero, A. Radi, S. Macke, R. Sutarto, F. He, G. A. Sawatzky, V. Hinkov, M. Kim, and H. N. Lee, Nano Lett. **12**, 4966 (2012).

[37] J. Fujioka, Y. Yamasaki, H. Nakao, R. Kumai, Y. Murakami, M. Nakamura, M. Kawasaki, and Y. Tokura, Phys. Rev. Lett. **111**, 027206 (2013).

[38] M. Karolak, M. Izquierdo, S. L. Molodtsov, and A. I. Lichtenstein, Phys. Rev. Lett. **115**, 046401 (2015).

[39] S. El-Khatib, D. Phelan, J. G. Barker, H. Zheng, J. F. Mitchell, and C. Leighton, Phys. Rev. B **92**, 060404(R) (2015).

[40] J. Badro, J. Rueff, G. Vanko, G. Monaco, G. Fiquet, and F. Guyot, Science **305**, 383 (2004).

[41] J. Li, V. V. Struzhkin, H.-k. Mao, J. Shu, R. J. Hemley, Y. Fei, B. Mysen, P. Dera, V. Prakapenka, and G. Shen, Proc. Natl. Acad. Sci. U.S.A. **101**, 14027 (2004).

[42] C. McCammon, I. Kantor, O. Narygina, J. Rouquette, U. Ponkratz, I. Sergueev, M. Mezouar, V. Prakapenka, and L. Dubrovinsky, Nat. Geosci. **1**, 684 (2008).

[43] J. -F Lin, H. Watson, G. Vanko, E. E. Alp, V. B. Prakapenka, P. Dera, V. Struzhkin, A. Kubo, J. Zhao, C. McCammon, and W. J. Evans, Nat. Geosci. **1**, 688 (2008).

[44] V. Potapkin, C. McCammon, K. Glazyrin, A. Kantor, I. Kupenko, C. Prescher, R. Sinmyo, G. V. Smirnov, A. I. Chumakov, R. Rüffer, and L. Dubrovinsky, Nat. Commun. **4**, 1427 (2013).

[45] H. Hsu, K. Umemoto, P. Blaha, and R. M. Wentzcovitch, Earth Planet. Sci. Lett. **294**, 19 (2010).

[46] H. Hsu, P. Blaha, M. Cococcioni, and R. M. Wentzcovitch, Phys. Rev. Lett. **106**, 118501 (2011).

[47] H. Hsu and R. M. Wentzcovitch, Phys. Rev. B **90**, 195205 (2014).

[48] Y. G. Yu, H. Hsu, M. Cococcioni, and R. M. Wentzcovitch, Earth Planet. Sci. Lett. **331–332**, 1 (2012).

[49] H. Hsu, Y. G. Yu, and R. M. Wentzcovitch, Earth Planet. Sci. Lett. **359–360**, 34 (2012).

[50] R. M. Wentzcovitch, H. Hsu, and K. Umemoto, Eur. J. Mineral. **24**, 851 (2012).

[51] I. S. Jacobs, J. Appl. Phys. **34**, 1106 (1963).

[52] V. Badaut, P. Zeller, B. Dorado, and M. L. Schlegel, Phys. Rev. B **82**, 205121 (2010).

[53] H. Shi, W. Luo, B. Johansson, and R. Ahuja, Phys. Rev. B **78**, 155119 (2008).

[54] D. M. Sherman, Am. Min. **94**, 166 (2009).

[55] See Supplemental Material at http://link.aps.org/supplemental/10.1103/PhysRevB.94.060404 for the computation method, high-resolution graph for the atomic structure, diagram for the orbital occupancy, electronic structure of the LS state, and the calculation of the iron nuclear QS.

[56] M. Cococcioni and S. de Gironcoli, Phys. Rev. B **71**, 035105 (2005).

[57] H. J. Kulik, M. Cococcioni, D. A. Scherlis, and N. Marzari, Phys. Rev. Lett. **97**, 103001 (2006).

[58] B. Himmetoglu, R. M. Wentzcovitch, and M. Cococcioni, Phys. Rev. B **84**, 115108 (2011).

[59] B. Himmetoglu, A. Floris, S. Gironcoli, and M. Cococcioni, Int. J. Quantum Chem. **114**, 14 (2014).

[60] K. Umemoto, H. Hsu, and R. M. Wentzcovitch, Phys. Earth Planet. In. **180**, 209 (2010).